analytical chemistry

Article

Cite This: *Anal. Chem.* 2019, 91, 5605−5612

pubs.acs.org/ac

Kinetic Understanding of the Ultrahigh Ionization Efficiencies (up to 28%) of Excited-State CH_2Cl_2-Induced Associative Ionization: A Case Study with Nitro Compounds

Jingyun Huang,[†,‡] Bo Yang,[*,†] Jinian Shu,[*,†,‡] Zuojian Zhang,[†,‡] Zhen Li,[†] and Kui Jiang[†,‡]

[†]National Engineering Laboratory for VOCs Pollution Control Material & Technology, University of Chinese Academy of Sciences, Beijing 101408, People's Republic of China

[‡]State Key Laboratory of Environment Simulation and Pollution Control, Research Center for Eco-Environmental Sciences, Chinese Academy of Sciences, Beijing 100085, People's Republic of China

Supporting Information

ABSTRACT: Excited-state CH_2Cl_2-induced associative ionization (AI) is a newly developed ionization method that is very effective for oxygenated organics. However, this method is not widely known. In this study, an unprecedented ionization efficiency and ultrafast reaction rate of AI toward nitro compounds were observed. The ionization efficiencies of *o*-nitrotoluene (o-NT), *m*-nitrotoluene (m-NT), and nitrobenzene (NB) were as high as (28 ± 3)%, (27 ± 2)%, and (13 ± 1)%, respectively (~1−3 ions for every 10 molecules). The measured reaction rate coefficients of these nitroaromatics were (0.5−1.3) × 10^{-7} molecule^{-1} cm^3 s^{-1} (~300 K). These unusual rate coefficients indicated strong long-range interactions between the two neutral reactants, which was regarded as a key factor leading to the ultrahigh ionization efficiency. The detection sensitivities of the nitroaromatics, (1.01−2.16) × 10^4 counts pptv^{-1} in 10 s acquisition time, were obtained by an AI time-of-flight mass spectrometer (AI-TOFMS). These experimental results not only provide new insight into the AI reaction but also reveal an excellent ionization method that can improve the detection sensitivity of nitroaromatics to an unprecedented degree.

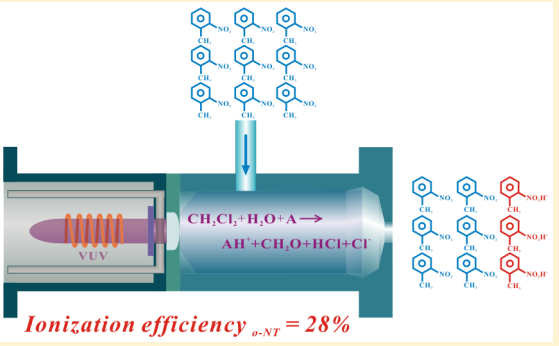

The ion source is the core part of a mass spectrometer (MS), and the efficiency of the ionization method used limits the detection sensitivity of the MS.[1] Although there are numerous configurations of ion sources, basic ionization methods are few. Major advances in ionization technology, such as the invention of new ionization methods, usually greatly promote the use of MSs in a specific field. Currently, the urgent need for real-time trace measurements in environmental analysis, security checks, disease diagnosis, etc. has led to a demand for new high-efficiency ionization methods to facilitate quick analyses and avoid time-consuming pretreatment procedures.

Gas-phase ionization technology is a fundamental ionization technology that can be used to ionize gaseous species directly or liquid/solid species via evaporation, nebulization, and laser desorption.[2] Electron ionization (EI) is a versatile conventional gaseous ionization technique that is widely used in chemical component analytical instruments, such as gas chromatograph−mass spectrometers (GC/MSs). EI ionizes molecules by impacting the gaseous analyte with a 70 eV electron beam (~mA), which usually operates at <10^{-2} Pa. The ionization efficiencies of typical EI ion sources are in the range of 10^{-6}−10^{-4} ion/molecule.[3] As the process is limited by insufficient ionization efficiency, enrichment via a pretreatment procedure is usually needed in the use of EI source-coupled MSs for trace measurements.

Single photon ionization (SPI) is another conventional gaseous ionization technique. SPI causes ionization by illuminating the gaseous analyte with vacuum ultraviolet (VUV) light under high vacuum. The efficiency of SPI depends on the photon flux of the VUV light, the photon ionization cross section of the analyte (10^{-18}−10^{-17} cm^2 molecule^{-1}),[4] and the interaction time. Theoretically, the efficiency of SPI can achieve 100% if the VUV light source is powerful enough. In fact, the typical photon fluxes of commercially available VUV lamps are approximately 10^{11}−10^{13} photons cm^{-2} s^{-1},[5] and the residence time of the analyte under high-vacuum conditions is very short, which causes the efficiency of conventional SPI sources to be extremely low. Low-pressure photoionization is a photoionization method performed under elevated pressure in the photoionization region (10^2−10^3 Pa).[5−7] With a remarkably increased residence time of the analyte in the photoionization region, the efficiency of low-pressure photoionization sources can be

Received: October 19, 2018
Accepted: March 6, 2019
Published: March 6, 2019

DOI: 10.1021/acs.analchem.8b04813
Anal. Chem. 2019, 91, 5605−5612

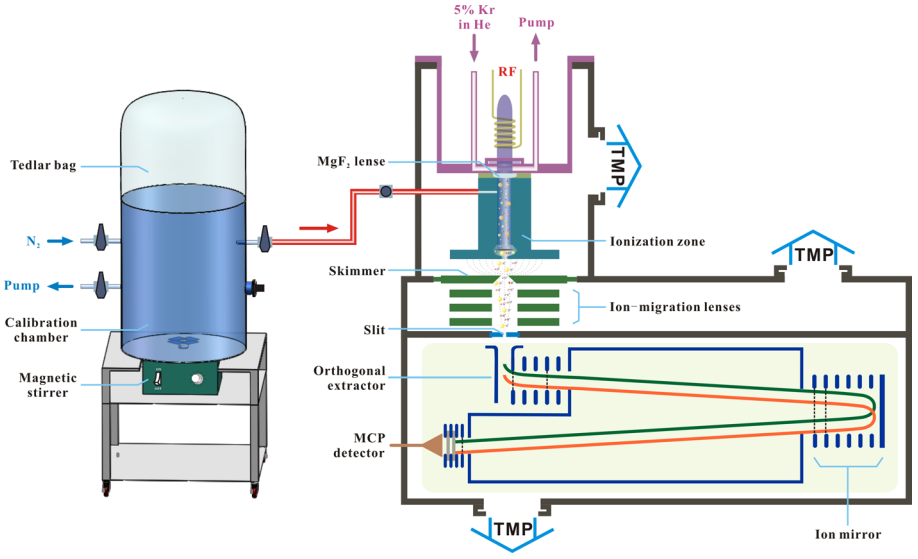

Figure 1. Schematic diagram of the calibration chamber and the AI ion source coupled with an orthogonal acceleration time-of-flight mass spectrometer.

improved relative to that of EI sources for some compounds, such as benzene and its derivatives. In addition, atmospheric pressure photoionization (APPI) is a unique photoionization technique developed for liquid chromatography−mass spectrometry (LC-MS) to detect molecules with lower polarity and volatility. The dominant ionization pathway of APPI involves the direct photoionization of a dopant or solvent (with ionization energy (IE) below the photon energy) to produce primary ions followed by charge exchange with the analyte.[8,9] The APPI process can be generally regarded as a chemical ionization (CI) process; thus, the overall ionization efficiency of APPI is likely similar to that of CI.

CI is a type of indirect ionization technique that ionizes a neutral analyte through a gas-phase ion−molecule reaction with an ionic reagent prepared in advance. The ionic reagent can be positive ions or negative ions, and CI is classified into positive chemical ionization (PCI) and negative chemical ionization (NCI) on the basis of the different ionic reagent involved. CI's ionization efficiency depends on the ion−molecule reaction rate, the concentration of reagent ions, and the reaction time. The rate constants of ion−molecule reactions are generally on the order of $\sim 10^{-9}$ molecule^{-1} cm^3 s^{-1}.[10] The ionization efficiency of a typical CI ion source is approximately $\sim 10^{-5}$ ion/molecule. Though the ionization efficiency of CI is not much higher than those of EI and SPI, the instrumental sensitivity of CI MS is greatly increased and benefits from the higher sample flow rates and longer reaction times. Moreover, resonance electron capture (REC) is an efficient negative ion formation pathway that is distinguished from the mechanism of NCI but may occur in an NCI ion source.[11,12] REC is a highly selective ionization method with particular sensitivity to the compounds containing electronegative elements. The rate constants of REC may reach 10^{-7} molecule^{-1} cm^{-3} s^{-1} for polyhalogenated compounds and 10^{-8} molecule^{-1} cm^{-3} s^{-1} for nitroaromatics at 125 °C.[11,13] These rate constants correspond to a sensitivity increase of 10−100 times in comparison with CI.

Penning ionization usually refers to the ionization of a target particle via collision with an excited atom/molecule and has been developed as an independent ion source technique for mass spectrometry. Sulimenkov et al.[14] and Verenchikov et al.[15] utilized high-density metastable Ar* atoms produced by glow discharge to ionize a neutral analyte, achieving absolute ionization efficiencies of 10^{-5} ion/molecule and 10^{-3} ion/molecule, respectively.

Complex ionization methods such as atmospheric pressure chemical ionization (APCI),[16−21] dielectric-barrier discharge ionization (DBDI),[22−25] and glow discharge[26,27] are also common ionization technologies that have been developed for the direct sensitive detection of volatile organic or inorganic compounds. In the process of complex ionization, all or parts of EI, SPI, CI, and Penning ionization may co-occur in the ionization region. Wolf et al. developed an active capillary DBDI MS for the direct measurement of chemical warfare agents, achieving a maximum sensitivity of 500 counts per second (cps)/pptv^{-1}.[25] The efficiency of this ionization method was roughly estimated to be $\sim 10^{-4}$ ion/molecule by assuming that the instrumental detection efficiency of the MS was $\sim 10^{-3}$.

Associative ionization (AI) is a gas-phase ionizing reaction that results from collisions between two neutral species (excited or not) and involves the formation of new bonds. Though AI occurs commonly in flames and plasma-based ionization processes,[2,28] it has rarely been used as an independent ionization source for mass spectrometry. In a recent study, a novel VUV-excited CH_2Cl_2-induced AI reaction was reported.[29] In this reaction, the gaseous CH_2Cl_2 molecule absorbs VUV light and forms excited ion-pair species, which then induce proton transfer from H_2O molecules to the analyte molecules with the aid of the reorganization energy released from the formation of CH_2O and HCl. The AI process is fundamentally different from dopant-assisted APPI and CI because both CH_2Cl_2 (IE, 11.3 eV) and H_2O (IE, 12.6 eV) cannot be ionized directly by the VUV light with photon energies of 10.0 and 10.6 eV. The ionization pathway involves neither direct photoionization nor an ion−molecule reaction. The new method presented an excellent ability to protonate oxygenated organics. The ionization efficiency toward oxygenated organics reached $\sim 10^{-3}$ ion/molecule. However, the intrinsic processes of AI were not well revealed.

DOI: 10.1021/acs.analchem.8b04813
Anal. Chem. 2019, 91, 5605−5612

Nitro-organic compounds are important environmental pollutants mainly derived from anthropogenic activities.[30] Many of these substances, especially nitroaromatics, have adverse human health effects, such as direct mutagenic activity and carcinogenicity.[31] In addition, nitroaromatics and nitroamines are well-known reactive components of prevalent explosives that may cause a serious threat to public security.[32] The marked increase in international terror incidents in recent years has given rise to increased research into explosive detection as well as the further exploration of new analytical techniques to enable faster, sensitive, and onsite determinations of nitro-organic compounds.[33−36] Nonetheless, the detection of nitroaromatic compounds in air is still one of the greatest remaining challenges due to the very low vapor pressures of such compounds.[37]

In the present study, the AI process of a series of nitro-organic compounds, including *o*-nitrotoluene (o-NT), *m*-nitrotoluene (m-NT), nitrobenzene (NB), nitromethane (NM), nitroethane (NE), and nitropropane (NP), in gaseous samples was investigated using AI coupled with a time-of-fight mass spectrometer (AI-TOFMS). The mass spectra, ionization efficiencies, and detection sensitivities of the nitro compounds were measured and analyzed. The ultrahigh ionization efficiencies of AI toward nitroaromatics were determined to be far greater than those obtained for the above-mentioned ionization methods.

EXPERIMENTAL SECTION

Chemicals and Gases. In this study, dichloromethane (99.9%, J&K), *o*-nitrotoluene (≥99.5%, Aladdin), *m*-nitrotoluene (99.0%, Aladdin), nitrobenzene (≥99.8%, Aladdin), nitropropane (98+%, Adamas), nitroethane (99%, Alfa), and nitromethane (98+%, Alfa) were used. High-purity nitrogen (>99.999%) was purchased from Beijing Haike Yuanchang Gas Co., Ltd. Krypton (5%, v/v) with helium as the balance gas was purchased from Beijing Huayuan Gas Co., Ltd.

Sample Preparation. A 60 L calibration chamber was used to generate defined gas-phase analyte concentrations, as shown in Figure 1. The calibration chamber was an open-head stainless-steel drum covered with a thin Tedlar bag (custom-built) to maintain a pressure of 1 atm. A magnetically driven fan was set at the bottom of the chamber to mix the gas species sufficiently. The inner temperature of the calibration chamber was maintained at ∼30 °C by two thermal radiation heaters outside the chamber. Before each experiment, the calibration chamber was filled with high-purity N_2 as a buffer gas. Then, 5 mL of pure CH_2Cl_2 liquid was injected into the calibration chamber, resulting in an equivalent gaseous concentration of 2.9×10^4 ppmv after evaporation. Similarly, gaseous samples were obtained by the volatilization of a certain amount of nitro-compound solution in the calibration chamber. To obtain a large range of gas-phase analyte concentrations (0.1−500 ppbv), three concentrations of sample solution (0.27, 2.7, and 27 mmol L^{-1}) with CH_2Cl_2 as a solvent were prepared. For each experiment, the total amount of solution injected into the chamber was less than 60 μL; hence, the influence of the solvent CH_2Cl_2 on the signal intensity of the analyte was ignored. The gaseous analyte was sampled by means of a stainless-steel tube, which was heated to ∼60 °C to minimize vapor loss.

Associative Ionization Source. The AI source was mainly composed of a VUV lamp and a cylindrical cavity (6 mm i.d., 30 mm long), which served as an ionization zone. The two components were coaxially connected through a MgF_2 lens, which was applied to focus VUV light into the ionization zone. VUV light was generated via the excitation of a mixed rare gas (5% krypton in helium) at ∼350 Pa using a 13.56 MHz radio frequency (rf) power supply running at 60 W. The output of the VUV lamp was $\sim 2 \times 10^{14}$ photons cm^{-2} s^{-1} with energies of 10.0 eV (80%) and 10.6 eV (20%). The pressure of the ionization zone was ∼1300 Pa when the sample flow rate was 2.8 cm^3 s^{-1}. The mixture of gas-phase CH_2Cl_2 and the analyte in the calibration chamber was sampled into the ionization zone and underwent an AI ionization reaction under the excitation of VUV light. The mechanism of the AI reaction was introduced in detail in a previous study.[29] CH_2Cl_2 was selected as a dopant to induce the AI reaction because CH_2Cl_2 cannot be ionized directly by the VUV light and fewer nontarget ions are produced in the ion source. Furthermore, CH_2Cl_2 has a more significant enhancing effect on the ion formation in comparison to some other chlorohydrocarbons. The gas-phase H_2O in the system was derived from water impurities in the high-purity N_2 and residual H_2O desorbed from the walls of the system. The concentration of gaseous H_2O inside the system was estimated to be 380 ppmv on the basis of the concentration calibrated by $H_2{}^{18}O$.[29] In the experiment performed to determine the ionization efficiency of the analyte, the ion current generated from the ion source was measured by a picoammeter (Keithley, Model 6485) with a gold-electroplated copper plate serving as the ion collector electrode, placed facing the outlet of the ionization zone. The ionizer was biased with an 8 V positive dc source to extract cations.

Mass Spectrometer. A detailed description of the MS has been given elsewhere.[7] Briefly, the ions ejected from the ion source were focused by a group of electrostatic ion lenses that were orthogonally connected to a V-shaped TOFMS with a flight distance of 460 mm. The mass resolution ($m/\Delta m$) of the TOFMS was ∼300 at m/z 78, and the acquisition time for each mass spectrum was 10 s. To protect the detector from waste, the signal intensity was reduced by setting a slit (0.2 mm × 1 mm) at the entry orifice of the TOF cavity and adjusting the voltages of the ion-migration lens assembly. Each method was performed three times to ensure the reproducibility of the signal reduction. The signal intensities shown in the paper have been corrected using the normal ion detection efficiency of the MS.

RESULTS AND DISCUSSION

AI Mass Spectra of Nitro Compounds. Excited CH_2Cl_2-induced AI is a new soft ionization technique with several unique mass spectrometric characteristics. As seen in Figure 2, which shows the AI mass spectra of 1 ppbv o-NT, m-NT, and NB, protonated molecular ions dominate the AI mass spectra, revealing high proton transfer efficiencies. The protonated molecular ions mainly include the protonated analyte (MH^+) and hydronium ions as well as the hydronium water clusters (H_3O^+, $(H_2O)_2H^+$, $(H_2O)_3H^+$, and $(H_2O)_4H^+$, with m/z values of 19, 37, 55, and 73, respectively). H_3O^+ was derived from the AI of residual H_2O in the ionization region, and its water clusters ($(H_2O)_nH^+$) mainly formed during the gas expansion process at the exit of the ion source. In addition, AI is inclined to produce more fragment ions in contrast to H_3O^+-induced PTR, partially due to its relatively excessive heat of reaction. The energetic calculation for NM, NE, and NB is shown in the Supporting Information. For the nitro compounds investigated, the major fragment ions were (M −

DOI: 10.1021/acs.analchem.8b04813
Anal. Chem. 2019, 91, 5605−5612

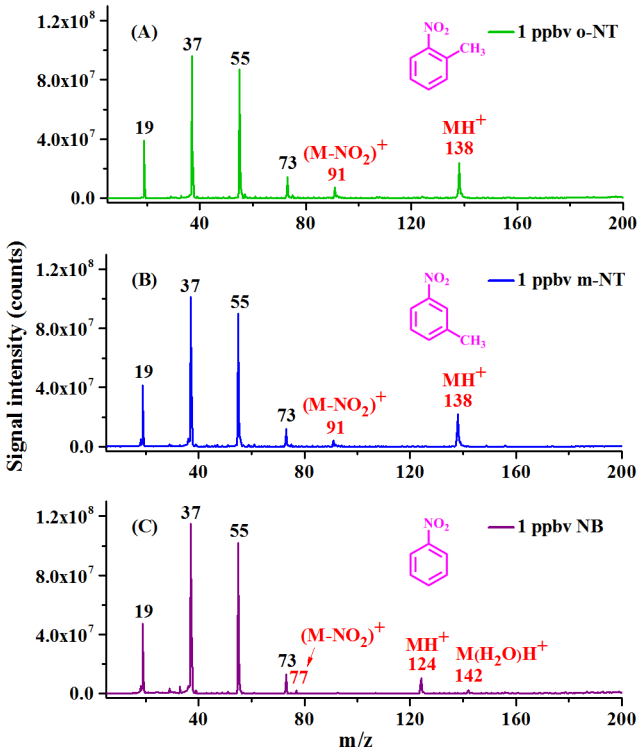

Figure 2. AI mass spectra of 1 ppbv o-NT (A), m-NT (B), and NB (C) in nitrogen.

$NO_2)^+$, indicating that the fragmentation pattern of AI is analogous to that of VUV photoionization. Most importantly, in contrast to many complex ionization methods, such as APCI and plasma-based ionization techniques, AI is a single ionization method involving only one ionization mechanism. Some of the greatest advantages of this ionization mode are substantially fewer background ions and fewer nontarget ions, which improve the detection limit and present a clear and concise mass spectrum for mixture analysis. AI mass spectra of the three nitroaliphatic compounds (NM, NE, and NP) are shown in Figure S1 of the Supporting Information, showing mass spectrum patterns similar to those of nitroaromatic compounds. These results reveal that AI is a promising ionization mode for application in mass spectrometry to directly characterize nitro-organic compounds in a gaseous matrix.

Ionization Efficiency of AI. Excited-state CH_2Cl_2-induced AI is a new ionization process, and the ionization efficiencies of common organics in this process have not yet been investigated and documented. Previous studies revealed that, in comparison with hydrocarbons, only oxygenated organics can be ionized efficiently by excited-state CH_2Cl_2-induced AI. Nitro compounds, which contain a NO_2 group via the C−N bond, belong to a special class of organics rather than the common oxygenated organics. In this paper, the absolute ionization efficiency of AI toward the nitro compounds, which was defined as the ratio of the flux of analyte ions emitted from the ion source (I_A, ions s^{-1}) to the flux of neutral molecules introduced (F_A, molecules s^{-1}), was determined using the equation

$$\text{ionization efficiency} = \frac{I_A}{F_A} = \frac{\frac{I}{e}R_A}{n_A q} \quad \text{(E1)}$$

where I is the total ion current measured by a picoammeter (A), e is the elementary charge (1.6×10^{-19} C), n_A is the gaseous concentration of analyte in the calibration chamber (molecules cm^{-3}), and q is the sampling flow rate of the instrument (2.8 cm^3 s^{-1}). R_A is the relative abundance of the analyte ions, which was calculated from the relative peak areas shown in the mass spectra and corrected by the relative transmission and detection efficiencies of individual m/z values. The correction method is shown in the Supporting Information. Parts A and B of Figure 3 respectively show the

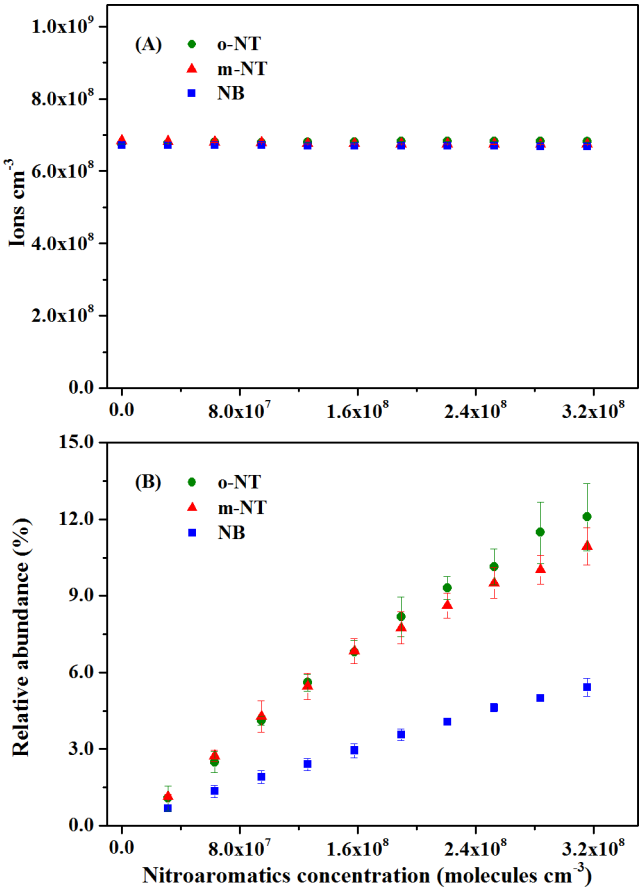

Figure 3. Dependence of the total ion intensity (A) and the relative abundance of analyte ions (B) on the partial flow rate of aromatic nitro compounds at a concentration of 0.1−1 ppbv in the calibration chamber.

total ion intensity (I/e) and the relative abundance of the analyte ions (R_A) versus the partial flow rate of the nitroaromatic compounds (F_A) in a concentration range of 0.1−1 ppbv. As shown in Figure 3, the total ion intensity showed little change, while the relative abundance of the analyte ions increased almost linearly with an increased number of analyte molecules, indicating a near-constant ionization efficiency for each compound within the calibration range. By using eq E1, the average ionization efficiencies of the six nitro-organic compounds were calculated, and they are shown in Table 1. The ionization efficiencies of o-NT, m-NT, and NB were measured to be (28 ± 3)%, (27 ± 2)%, and (13 ± 1)%, respectively. In other words, the ion source generated ~10^7 ions $pptv^{-1}$ s^{-1} toward these compounds. The observed ultrahigh efficiency of AI toward nitroaromatics indicates a

DOI: 10.1021/acs.analchem.8b04813
Anal. Chem. 2019, 91, 5605−5612

Table 1. AI Efficiencies and Reaction Rate Coefficients of the Nitro Compounds Investigated[a]

compound	ionization efficiency (%)	concentration range (ppbv)	reaction rate coefficient, k (molecules^{-1} cm^3 s^{-1})
o-NT	28 ± 3	0.1−1	1.3×10^{-7}
m-NT	27 ± 2	0.1−1	1.2×10^{-7}
NB	13 ± 1	0.1−1	5.0×10^{-8}
NP	1.3 ± 0.2	0.5−10	5.9×10^{-9}
NE	0.86 ± 0.09	0.5−10	3.6×10^{-9}
NM	0.24 ± 0.03	10−30	7.5×10^{-10}

[a]The uncertainty shown in Table 1 was obtained from three parallel experiments.

potential unprecedented advance in detection technology in certain fields.

Reaction Rate Coefficient of AI. To interpret the ultrahigh ionization efficiency obtained, the rate coefficients of the AI reaction toward these nitro-organic compounds were investigated. The relevant reactions in the ion source are

$$CH_2Cl_2 \underset{k_{-1}}{\overset{k_1}{\rightleftarrows}} CH_2Cl_2^* \quad \text{(R1)}$$

$$CH_2Cl_2^* + H_2O \xrightarrow{k_2} RC \quad \text{(R2)}$$

$$RC + A \xrightarrow{k_A} AH^+ + CH_2O + HCl + Cl^- \quad \text{(R3)}$$

$$RC + H_2O \xrightarrow{k_{H_2O}} H_3O^+ + CH_2O + HCl + Cl^- \quad \text{(R4)}$$

where RC represents the reaction complex [H_2O−CH_2Cl^+−Cl^-], which is regarded as the reactant that interacts with the analyte to perform the AI reaction. Since CH_2Cl_2* and RC are unstable intermediates, under the steady-state approximation, their rate equations can be expressed as

$$\frac{d[CH_2Cl_2^*]}{dt} = k_1[CH_2Cl_2] - k_{-1}[CH_2Cl_2^*] - k_2[CH_2Cl_2^*][H_2O] = 0 \quad \text{(E2)}$$

$$\frac{d[RC]}{dt} = k_2[CH_2Cl_2^*][H_2O] - k_{H_2O}[RC][H_2O] - k_A[RC][A] = 0 \quad \text{(E3)}$$

From eqs E2 and E3, we can obtain [RC] from

$$[RC] = \frac{k_1[CH_2Cl_2] - k_{-1}[CH_2Cl_2^*]}{k_{H_2O}[H_2O] + k_A[A]} \quad \text{(E4)}$$

Then, the rate equation of the analyte ion (AH^+) is described by

$$\frac{d[AH^+]}{dt} = k_A[RC][A] = \frac{k_A[A](k_1[CH_2Cl_2] - k_{-1}[CH_2Cl_2^*])}{k_{H_2O}[H_2O] + k_A[A]} \quad \text{(E5)}$$

Given $[A] = [A]_0 - [AH^+]$, the definite integral of the rate formula E5 can be written as

$$k_{H_2O}[H_2O] \ln \frac{[A]_0}{[A]_0 - [AH^+]} + k_A[AH^+] = k_A(k_1[CH_2Cl_2] - k_{-1}[CH_2Cl_2^*])t \quad \text{(E6)}$$

where $[A]_0$ and $[AH^+]$ are the initial concentration of analyte A and the produced ion concentration of AH^+, respectively, which are calculated from F_A and I_A divided by the gas flow rate inside the ion source (218 cm^3 s^{-1}, estimated with the pressure of ion source (P_I, 1300 Pa), the sample flow rate of the instrument (q, 2.8 cm^3 s^{-1}), and one atmospheric pressure (P_A, 101325 Pa) using the formulation $q \times P_A/P_I$), t is the ionization reaction time, i.e., the residence time of the analyte (3.9×10^{-3} s), $k_1[CH_2Cl_2] - k_{-1}[CH_2Cl_2^*]$, which represents the net generation rate of reactive CH_2Cl_2*, is determined to be 1.7×10^{11} molecules cm^{-3} s^{-1}, and the value of $k_{H_2O}[H_2O]$ is considered to be larger than 256 s^{-1} (the derivation of the last two parameters can be seen in the Supporting Information). Thus, by fitting the data points of $[AH^+]$ versus $[A]_0$ with eq E6, as shown in Figure 4, the AI reaction rate coefficient for the analyte, k_A, was obtained. Nonlinear curve fitting and regression were performed with the software *1stopt1.5* using the Levenberg−Marquardt algorithms. The corresponding rate coefficients for the nitro compounds investigated ranged from 7.5×10^{-10} to 1.3×10^{-7} molecule^{-1} cm^3 s^{-1}, as shown in Table 1. It should be noted that the

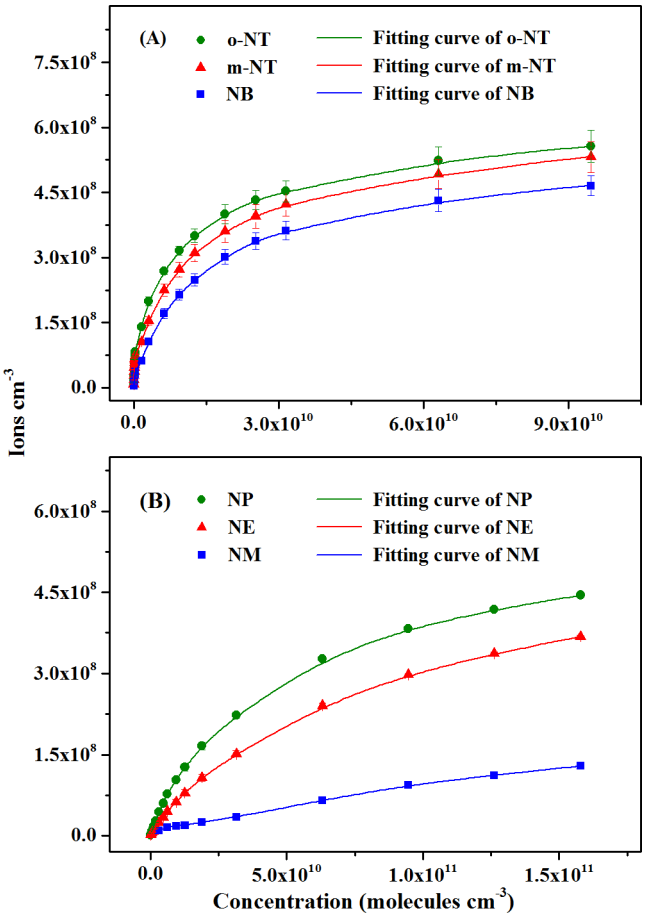

Figure 4. Dependence of ion concentration on the molecular concentration of aromatic nitro compounds (A) and aliphatic nitro compounds (B) in the ionization region.

DOI: 10.1021/acs.analchem.8b04813
Anal. Chem. 2019, 91, 5605−5612

reaction rate coefficients obtained in this study may be underestimated to a certain degree due to the underestimation of the value of $k_{H_2O}[H_2O]$.

The obtained AI reaction rates of nitroaromatics ($(0.5-1.3) \times 10^{-7}$ molecule^{-1} cm^3 s^{-1}) are substantially faster than the barrierless neutral−neutral reaction limit described by the notional hard sphere model and are 2 orders of magnitude higher than those of long-range ion−molecule reactions ($\sim 10^{-10}-10^{-9}$ molecule^{-1} cm^3 s^{-1}).[10] Thus, the obtained AI reaction rate constants indicate an unusual long-range dipole−dipole attractive force between the reactants. These rate constants imply that, with a mean relative velocity of 350 m s^{-1} at 300 K, the effective collision radius between reactants would be 68−109 Å. This feature is very similar to some other AI reactions available in the literature. The rate constants of fast AI reactions have been reported on the order of $\sim 10^{-10}-10^{-9}$ molecule^{-1} cm^3 s^{-1} at ∼300 K,[38−41] and the rate constants of certain AI reactions, e.g., highly excited Na atoms with the electronegative molecule SF_6, can achieve 10^{-7} molecule^{-1} cm^3 s^{-1} at room temperature.[42] Notably, these AI reactions are initiated by the effects of excited-state noble gases or metallic atoms.[43−46] As far as we know, excited-state organic-induced AI reactions have never been reported, with the exception of the newfound excited-state CH_2Cl_2-induced ionization reaction.[29] Further investigations into the dynamic mechanism of this AI reaction are necessary for understanding this valuable chemical process.

Sensitivity and LODs of AI-TOFMS. The detection sensitivities of the present AI-TOFMS were determined by linear fitting of the signal intensities of the protonated molecular ion responses to varying concentrations of analyte, as shown in Figure S2. Error bars were calculated from three parallel experiments. The fitting results for the data points are shown in Table 2. Good linear relationships were obtained with correlation coefficients (R^2) ranging from 0.9882 to 0.9995 within the calibrated range. The slopes of the fitted lines were defined as the detection sensitivities, which ranged from 92.6 ± 4.5 to $(2.16 \pm 0.05) \times 10^4$ counts pptv^{-1} in a 10 s acquisition time. It is reported that the proton transfer reaction−mass spectrometer (PTR-MS), which is one type of commercial CI MS used for the real-time measurement of trace volatile organics,[47−52] has a maximum sensitivity of 4.7 cps/pptv at a sample rate of 8.3 cm^3 s^{-1}.[47] In addition, the reported sensitivities of typical high-sensitivity CI MS can reach dozens to hundreds of cps pptv^{-1} when the gas pressure of the ion source is $\sim 10^4-10^5$ Pa and the sample rate is increased to $\sim 10^2-10^3$ cm^3 s^{-1}.[53−55] In this experiment, the sensitivities of AI-TOFMS toward nitroaromatic compounds achieved thousands of cps pptv^{-1} at a low sample rate of only 2.8 cm^3 s^{-1}.

Table 2. Sensitivities of the Nitro Compounds Investigated

compound	sensitivity (counts/pptv)	correlation coefficient (R^2)	concentration range (ppbv)
o-NT	$(2.15 \pm 0.02) \times 10^4$	0.9995	0.1−1
m-NT	$(2.16 \pm 0.05) \times 10^4$	0.9947	0.1−1
NB	$(1.01 \pm 0.02) \times 10^4$	0.9969	0.1−1
NP	$(1.15 \pm 0.01) \times 10^3$	0.9984	2−100
NE	$(8.43 \pm 0.01) \times 10^2$	0.9988	2−100
NM	92.6 ± 4.5	0.9882	10−100

To obtain the directly measured LODs of nitroaromatic compounds, a pulsed microchannel plate detector was used to screen high-flux H_3O^+ and its cluster ions. The technical method and the schematic diagram of the experimental device are shown in the Supporting Information. Figure S3 shows the enlarged mass spectra of the ions generated from 10 pptv o-NT, 10 pptv m-NT, and 20 pptv NB, indicating that the directly measured LODs of nitroaromatics under the present experimental conditions are roughly at the 10 pptv level. The measured LOD is equivalent to ∼1.7 picograms (pg) for NT in 10 s acquisition time, calculated with the sample flow fate (2.8 cm^3/s^{-1}), the sample time (10 s), and the concentration of nitroaromatics (10 pptv).

At present, negative chemical ionization (NCI) and APPI ion sources are usually applied in GC-MS and LC-MS, respectively, for the off-line analysis of nitroaromatic samples, with LODs at a few picograms to hundreds of picograms.[56−59] In contrast, the directly measured LODs in this experiment are not greatly superior to those obtained by NCI and APPI, though the ionization efficiency of the AI method is much higher than those of NCI and APPI. The main reason for this result is that the present MS system (a simple V-shaped TOF) lacks a mass-selected function. Large amounts of H_3O^+ and its cluster ions swarming into the ion migration and detection region lead to a significant increase in background signals. In comparison, commercial NCI and APPI are usually equipped with quadrupole (Q) or QTOF mass spectrometers, which can selectively detect target ions and effectively reduce detection limits. On the basis of the AI efficiencies and reaction rate constants measured, we believe that the LOD of the proposed method would be more remarkable with an improvement in the mass spectrometer.

Applicability Discussion. Every gaseous ionization method has its corresponding applicable analytical field. Because almost all neutral analytes can be ionized by high-energy electrons (70 eV) or form positive ions through ion−molecule reactions, EI and PCI are considered to be universal ionization techniques. Traditional SPI is capable of ionizing the substances with IEs below the photon energy (usually ∼10 eV), and APPI applied in LC-MS is often used to detect hydrocarbons and organics with higher molecular weight. By comparison, NCI is a more selective ionization technique, which can be used for the analysis of compounds containing acidic groups or electronegative elements (especially halogens). The present AI method has been proved to be sensitive to common oxygenated organics and anilines.[29,60] On the basis of our experimental results, the reactivity of the AI reaction generally shows positive correlations with the polarizability, permanent dipole moment, and molar weight of the analyte,[61] which is consistent with the properties of long-range ion−molecule reactions.[62] Therefore, we speculate that the present ionization approach may have excellent performance for compounds with higher polarizabilities, permanent dipole moments, and molar weights, especially for polar organics with a delocalized system enhanced by electron-attracting/-donating functional groups, such as nitroaromatics, organophosphates, sulfonates, etc. Since most of these compounds are environmental contaminants, pesticides, explosives, and chemical warfare agents, this AI method may have great application prospects in the analysis of environmental and security-related samples. In addition, this AI phenomenon was just observed a few years ago, and its practicality remains to be explored by more researchers.

DOI: 10.1021/acs.analchem.8b04813
Anal. Chem. 2019, 91, 5605−5612

CONCLUSIONS

In this study, the ultrahigh ionization efficiency of a novel AI ion source toward organic nitro compounds was investigated with an AI-TOFMS. The reaction rate constants (7.5×10^{-10} to 1.3×10^{-7} molecule^{-1} cm^3 s^{-1}) of AI toward organic nitro compounds were obtained by analyzing the ion intensities and ion abundances. To the best of our knowledge, this is the first time that an excited-state organic-molecule-induced AI reaction rate has been measured and reported, especially such a high reaction rate ($\sim 10^{-7}$ molecule^{-1} cm^3 s^{-1}). The ultrahigh rate constant indicates a long-range attractive force between the reactants and a new chemical behavior of the excited-state organics. The intrinsic physical and chemical interactions of this AI reaction remain to be explored. With the aid of the efficient AI reaction, ultrahigh ionization efficiencies of nitroaromatic compounds were observed, with values of (28 ± 3)%, (27 ± 2)%, and (13 ± 1)% for o-NT, m-NT, and NB, respectively. The ionization efficiencies of AI toward these nitroaromatic compounds are $\sim 10^4$ times higher than those of CI. The $\sim 10^4$ gain in ionization efficiency can be roughly attributed to an $\sim 10^2$ contribution from the fast reaction rates of AI and an $\sim 10^2$ contribution from the high-concentration neutral reactant (excited-state CH_2Cl_2). In addition, the homogeneous mixing at the molecular level between excited-state CH_2Cl_2 and analytes in the ionization region is regarded as another important factor that may contribute to the ultrahigh ionization efficiency. When the photon flux of the VUV lamp is enhanced or the gas pressure of the ion source is increased, a 100% ionization efficiency of AI can be expected. The results of this investigation will hopefully prompt a tremendous advance in detection technology in related fields.

ASSOCIATED CONTENT

Supporting Information

The Supporting Information is available free of charge on the ACS Publications website at DOI: 10.1021/acs.analchem.8b04813.

Materials and methods and supplementary text, figures, and tables (PDF)

AUTHOR INFORMATION

Corresponding Authors

*E-mail for B.Y.: boyang@rcees.ac.cn.
*E-mail for J.S.: jshu@rcees.ac.cn.

ORCID

Bo Yang: 0000-0001-8090-4939
Jinian Shu: 0000-0002-6360-6953

Notes

The authors declare no competing financial interest.

ACKNOWLEDGMENTS

This study was supported by the National Natural Science Foundation of China (Grant Nos. 21527901 and 21777170) and the Beijing Municipal Science & Technology Commission (Z181100003818008).

REFERENCES

(1) Cheng, K.; Wong, C.; Wang, M.; He, Q.; Chen, F. *Mass Spectrom. Rev.* **2009**, *29*, 126−155.
(2) Bhardwaj, C.; Hanley, L. *Nat. Prod. Rep.* **2014**, *31*, 756−767.
(3) Vigne, S.; Alava, T.; Tassetti, C. M.; Duraffourg, L.; Progent, F. *Sens. Actuators, B* **2017**, *243*, 690−695.
(4) Kanno, N.; Tonokura, K. *Appl. Spectrosc.* **2007**, *61*, 896−902.
(5) Wang, Y.; Jiang, J.; Lei, H.; Hou, K.; Xie, Y.; Ping, C.; Wei, L.; Li, Q.; Shuang, W.; Li, H. *Anal. Chem.* **2016**, *88*, 9047−9055.
(6) Liu, C.; Zhu, Y.; Zhou, Z.; Yang, J.; Qi, F.; Pan, Y. *Anal. Chim. Acta* **2015**, *891*, 203−210.
(7) Sun, W.; Shu, J.; Zhang, P.; Li, Z.; Li, N.; Liang, M.; Yang, B. *Atmos. Meas. Tech.* **2015**, *8*, 4637−4643.
(8) Kauppila, T. J.; Syage, J. A.; Benter, T. *Mass Spectrom. Rev.* **2017**, *36*, 423−449.
(9) Klee, S.; Derpmann, V.; Wißdorf, W.; Klopotowski, S.; Kersten, H.; Brockmann, K. J.; Benter, T.; Albrecht, S.; Bruins, A. P.; Dousty, F.; Kauppila, T. J.; Kostiainen, R.; O'Brien, R.; Robb, D. B.; Syage, J. A. *J. Am. Soc. Mass Spectrom.* **2014**, *25*, 1310−1321.
(10) Faure, A.; Vuitton, V.; Thissen, R.; Wiesenfeld, L.; Dutuit, O. *Faraday Discuss.* **2010**, *147*, 337−348.
(11) Budzikiewicz, H. *Mass Spectrom. Rev.* **1986**, *5*, 345−380.
(12) Chernetsova, E. S.; Revelsky, A. I.; Revelsky, I. A.; Mikhasenko, I. A.; Sobolevsky, T. G. *Mass Spectrom. Rev.* **2002**, *21*, 373−387.
(13) Knighton, W. B.; Mock, R. S.; McGrew, D. S.; Grimsrud, E. P. *J. Phys. Chem.* **1994**, *98*, 3770−3776.
(14) Sulimenkov, I. V.; Brusov, V. S.; Zelenov, V. V.; Skoblin, M. G.; Filatov, V. V.; Pikhtelev, A. R.; Kozlovskii, V. I. *J. Anal. Chem.* **2017**, *72*, 1331−1339.
(15) Verenchikov, A. N.; Kolosov, A. P. *J. Anal. Chem.* **2015**, *70*, 1527−1532.
(16) Heaney, L. M.; Ruszkiewicz, D. M.; Arthur, K. L.; Hadjithekli, A.; Aldcroft, C.; Lindley, M. R.; Thomas, C. P.; Turner, M. A.; Reynolds, J. C. *Bioanalysis* **2016**, *8*, 1325−1336.
(17) Badjagbo, K.; Furtos, A.; Alaee, M.; Moore, S.; Sauvé, S. *Anal. Chem.* **2009**, *81*, 7288−7293.
(18) Jost, C.; Sprung, D.; Kenntner, T.; Reiner, T. *Int. J. Mass Spectrom.* **2003**, *223−224*, 771−782.
(19) Sabo, M.; Matejčík, Š. *Analyst* **2013**, *138*, 6907−6912.
(20) Le Quere, J.-L.; Gierczynski, I.; Sémon, E. *J. Mass Spectrom.* **2014**, *49*, 918−928.
(21) O'Sullivan, D. W.; Silwal, I. K. C.; Mcneill, A. S.; Treadaway, V.; Heikes, B. G. *Int. J. Mass Spectrom.* **2018**, *424*, 16−26.
(22) Chen, L. C.; Yu, Z.; Hiraoka, K. *Anal. Methods* **2010**, *2*, 897−900.
(23) Hu, J.; Li, W.; Zheng, C.; Hou, X. *Appl. Spectrosc. Rev.* **2011**, *46*, 368−387.
(24) Yang, T.; Gao, D.; Yu, Y.; Chen, M.; Wang, J. *Talanta* **2016**, *146*, 603−608.
(25) Wolf, J. C.; Schaer, M.; Siegenthaler, P.; Zenobi, R. *Anal. Chem.* **2015**, *87*, 723−729.
(26) Bouza, M.; Fandino, J.; Bordel, N.; Pereiro, R.; Sanzmedel, A. *J. Mass Spectrom.* **2017**, *52*, 561−570.
(27) Nunome, Y.; Kodama, K.; Ueki, Y.; Yoshiie, R.; Naruse, I.; Wagatsuma, K. *Spectrochim. Acta, Part B* **2018**, *139*, 44−49.
(28) Martínez-Jarquín, S.; Winkler, R. *TrAC, Trends Anal. Chem.* **2017**, *89*, 133−145.
(29) Yang, B.; Zhang, H.; Shu, J.; Ma, P.; Zhang, P.; Huang, J.; Li, Z.; Xu, C. *Anal. Chem.* **2018**, *90*, 1301−1308.
(30) Marvinsikkema, F. D.; de Bont, J. A. *Appl. Microbiol. Biotechnol.* **1994**, *42*, 499−507.
(31) Lang, P.; Ma, X.; Lu, G.; Wang, Y.; Bian, Y. *Chemosphere* **1996**, *32*, 1547−1552.
(32) Akhgari, F.; Fattahi, H.; Oskoei, Y. M. *Sens. Actuators, B* **2015**, *221*, 867−878.
(33) Forbes, T. P.; Sisco, E. *Analyst* **2018**, *143*, 1948−1969.
(34) Meaney, M. S.; Mcguffin, V. L. *Anal. Chim. Acta* **2008**, *610*, 57−67.
(35) Jiang, D.; Peng, L.; Wen, M.; Zhou, Q.; Chen, C.; Wang, X.; Chen, W.; Li, H. *Anal. Chem.* **2016**, *88*, 4391−4399.
(36) Martínez-Lozano, P.; Rus, J.; Mora, G. F. D. L.; Hernández, M.; Mora, J. F. D. L. *J. Am. Soc. Mass Spectrom.* **2009**, *20*, 287−294.

DOI: 10.1021/acs.analchem.8b04813
Anal. Chem. 2019, 91, 5605−5612

(37) Ewing, R. G.; Waltman, M. J.; Atkinson, D. A.; Grate, J. W.; Hotchkiss, P. J. *TrAC, Trends Anal. Chem.* **2013**, *42*, 35−48.
(38) Brandao, J.; Rio, C. M. A. *J. Chem. Phys.* **2003**, *119*, 3148−3159.
(39) Ard, S. G.; Shuman, N. S.; Martinez, O.; Armentrout, P. B.; Viggiano, A. A. *J. Chem. Phys.* **2016**, *145*, 084302.
(40) Sheverev, V. A.; Stepaniuk, V. P.; Lister, G. G. *J. Appl. Phys.* **2002**, *92*, 3454−3457.
(41) Ard, S. G.; Shuman, N. S.; Martinez, O.; Brumbach, M. T.; Viggiano, A. A. *J. Chem. Phys.* **2015**, *143*, 204303.
(42) Beterov, I. M.; Vasilenko, G. L.; Riabtsev, I. I.; Smirnov, B. M.; Fateyev, N. V. *Z. Phys. D: At., Mol. Clusters* **1987**, *7*, 55−63.
(43) Fontijn, A. *Pure Appl. Chem.* **1974**, *39*, 287−306.
(44) Klucharev, A. N.; Vujnović, V. *Phys. Rep.* **1990**, *185*, 55−81.
(45) Mihajlov, A. A.; Srećković, V. A.; Ignjatović, L. M.; Klyucharev, A. N. *J. Cluster Sci.* **2012**, *23*, 47−75.
(46) Cannon, M.; Dunning, F. B. *J. Chem. Phys.* **2009**, *130*, 044304.
(47) Sulzer, P.; Hartungen, E.; Hanel, G.; Feil, S.; Winkler, K.; Mutschlechner, P.; Haidacher, S.; Schottkowsky, R.; Gunsch, D.; Seehauser, H. *Int. J. Mass Spectrom.* **2014**, *368*, 1−5.
(48) Hansel, A.; Jordan, A.; Holzinger, R.; Prazeller, P.; Vogel, W.; Lindinger, W. *Int. J. Mass Spectrom. Ion Processes* **1995**, *149*, 609−619.
(49) Yuan, B.; Koss, A.; Warneke, C.; Gilman, J. B.; Lerner, B. M.; Stark, H.; de Gouw, J. A. *Atmos. Meas. Tech.* **2016**, *9*, 2735−2752.
(50) de Gouw, J. D.; Warneke, C. *Mass Spectrom. Rev.* **2007**, *26*, 223−257.
(51) Lindinger, W.; Hansel, A.; Jordan, A. *Chem. Soc. Rev.* **1998**, *27*, 347−354.
(52) Blake, R. S.; Patel, M.; Monks, P. S.; Ellis, A. M.; Inomata, S.; Tanimoto, H. *Int. J. Mass Spectrom.* **2008**, *278*, 15−19.
(53) Lavi, A.; Vermeuel, M. P.; Novak, G. A.; Bertram, T. H. *Atmos. Meas. Tech.* **2018**, *11*, 3251−3262.
(54) Yao, L.; Wang, M.; Wang, X.; Liu, Y.; Chen, H.; Zheng, J.; Nie, W.; Ding, A.; Geng, F.; Wang, D.; Chen, D.; Worsnop, D. R.; Wang, L. *Atmos. Chem. Phys.* **2016**, *16*, 14527−14543.
(55) Zheng, J.; Khalizov, A.; Wang, L.; Zhang, R. *Anal. Chem.* **2010**, *82*, 7302−7308.
(56) Bamford, H. A.; Baker, J. E. *Atmos. Environ.* **2003**, *37*, 2077−2091.
(57) Lung, S. C. C.; Liu, C. H. *Sci. Rep.* **2015**, *5*, 12992.
(58) Song, L.; Wellman, A. D.; Yao, H.; Bartmess, J. E. *J. Am. Soc. Mass Spectrom.* **2007**, *18*, 1789−1798.
(59) Li, L.; Hang, H. S. S.; Ming, H. Y.; Chow, J. C.; Watson, J. G.; Liqin, W.; Linli, Q.; Junji, C. *Atmos. Environ.* **2018**, *192*, 84−93.
(60) Zhang, H.; Shu, J.; Yang, B.; Zhang, P.; Ma, P. *Talanta* **2018**, *178*, 636−643.
(61) Yang, B.; Xu, C.; Shu, J.; Li, Z.; Zhang, H.; Ma, P. *Talanta* **2019**, *194*, 888−894.
(62) Sekimoto, K.; Li, S. M.; Yuan, B.; Koss, A.; Coggon, M.; Warneke, C.; Gouw, J. D. *Int. J. Mass Spectrom.* **2017**, *421*, 71−94.

DOI: 10.1021/acs.analchem.8b04813
Anal. Chem. 2019, 91, 5605−5612